Climate Modelling User Group [CMUG]

Deliverable D2.0f v2

Interim progress report for OWP5.6 – Snow dynamics impacts on temperate / high latitude climate

Centres providing input: IPSL (LSCE)

Version nr.	Date	Status
2.1	07 May 2026	Input from partners
2.2	19 May 2026	Submitted to ESA

Deliverable 2.0f v2

Interim progress report for OWP5.6 - Snow dynamics impacts on temperate / high latitude climate

Authors: A. Cuynet, C. Ottlé

Contents

Interim progress report - Snow dynamics impacts on temperate / high latitude climate

1. Introduction – Purpose and scope of the report

This document is the technical report on the work carried out in the WP5.6 study of the CCI-CMUG project. Our study aims to improve the representation of snow cover dynamics in temperate and boreal zones within the IPSL climate model, using the snow cover fraction and snow water equivalent products recently released by the CCI Snow project (covering the last four decades), to assess the impact of snow cover dynamics and atmospheric feedback on regional to continental climate.

Snow cover plays a key role in the climate system through its strong control on surface albedo and energy exchanges between the land and the atmosphere. The presence, persistence, and radiative properties of snow are known to significantly affect the surface energy balance, particularly in mid- and high-latitude regions (Krinner et al., 2018; Betts et al. 2014). In this context, the snow cover fraction (SCF) and snow albedo are critical variables in land surface models (LSMs).

Vegetation has a major influence on both snow accumulation and radiative properties (Niu and Yang, 2004, Broxton et al., 2015). For instance, forests can intercept snowfall, reduce snow accumulation at the ground, and alter the surface albedo through canopy shading and radiative transfer processes. In contrast, low vegetation or bare soil allows snow to accumulate more uniformly and tends to exhibit higher and more homogeneous albedo values (Broxton et al., 2015, Alessandri et al., 2021). As a result, the interaction between snow and vegetation introduces strong spatial variability that is challenging to represent in LSMs.

In the ORCHIDEE LSM (version 4.3), snow processes are already represented, but the dependence of snow albedo and SCF on vegetation remains simplified. In particular, snow cover is computed at the grid-cell level using averaged properties, and the same SCF is applied to all plant functional types (PFTs) within a grid cell. This approach neglects important sub-grid variability related to land cover and may lead to significant biases, especially in heterogeneous landscapes.

The objective of this study is to improve the representation of snow albedo and SCF in ORCHIDEE by introducing a vegetation-dependent parameterisation. This involves (i) modifying the model equations to explicitly account for vegetation effects, and (ii) calibrating the associated parameters for each PFT using satellite observations. The calibration relies on multiple datasets, including CCI Snow products (SCFG, SCFV, and SWE) and MODIS albedo. Given the high computational cost of global optimisation and the complexity of mixed-vegetation grid cells, a site-based calibration strategy is adopted. Representative sites are selected for each PFT using a dedicated methodology designed to maximise data availability while ensuring spatial representativeness. The resulting parameter sets are then evaluated both at site level and at the global scale.

2. ORCHIDEE Land Surface Model

2.1 General description

In this study, simulations were performed using the ORCHIDEE Land Surface Model (Krinner et al., 2005). Version 4.3 of the model was used, which constitutes a stable branch incorporating the most recent developments. The ORCHIDEE v4.3 tag is employed within the Institut Pierre-Simon Laplace (IPSL) Earth System Model (IPSL-CM7), one of the models contributing to the Coupled Model Intercomparison Project CMIP-7 Fast Track (WCRP, 2026).

The model simulates the energy and water transfers in the soil-atmosphere continuum and at the surface-atmosphere interface, as well as the carbon and nitrogen cycles and their interactions (Vuichard et al., 2019). Vegetation processes are parameterized for 15 different Plant Functional Types (PFTs) presented in Table 1, related to their phenology, leaf type, physiological activity (e.g. C3/C4 photosynthetic pathways) and climate (Harper et al., 2023). Soil mineral composition is defined at the grid-cell level, based on the 12-classes of USDA soil classification (Forbes et al., 1987). While energy and snow processes are computed at the grid-cell scale (one energy budget for the whole cell), water processes are resolved by accounting for the PFTs present in the grid cell, with a maximum of three soil columns separating bare soil from high (e.g., forests) and low (e.g., grasslands) vegetation. Carbon stocks and fluxes are resolved for each PFT present within the grid cell. Different vertical grids are considered depending on the biogeophysical cycles considered. Soil hydrology and thermics share the same grid consisting of 11 layers from the surface and down to 2 m with a geometrically increasing internode distance. Thermal processes are resolved deeper, up to a maximum depth of 90 m, with 7 additional layers and a number of layers of 18 in the standard version. All thermal and hydrological properties are calculated according to soil composition (mineral, carbon and water components), accounting for soil freezing and snow thermo-hydric processes.

ORCHIDEE can be run at various scales ranging from local to global. For the present study, the model requires the prescription of the atmospheric conditions (air pressure, temperature and humidity, wind speed and incoming radiation), a description of the land surface (fraction of the different PFTs, dominant soil texture) and the initialization of the energy, water, carbon and nitrogen stocks. These conditions are derived from global datasets (i.e., atmospheric reanalysis, land cover and soil texture classifications) or from stand-level measurements.

PFT1: Bare Soil
PFT2: Tropical Evergreen
PFT3: Tropical Raingreen
PFT4: Temperate Needleleaf Evergreen
PFT5: Temperate Broadleaf Evergreen
PFT6: Temperate Broadleaf Summergreen
PFT7: Boreal Needleleaf Evergreen
PFT8: Boreal Broadleaf Summergreen
PFT9: Boreal Needleleaf Deciduous
PFT10: Temperate Natural Grassland (C3)
PFT11: Natural Grassland (C4)

PFT12: Crops (C3)
PFT13: Crops (C4)
PFT14: Tropical Natural Grassland (C3)
PFT15: Boreal Natural Grassland (C3)

Table 1: The 15 Plant Functional Types used in the ORCHIDEE model to describe vegetation

2.2 ORCHIDEE v4.3 – Snow model

The work performed in WP5.6 aims to use the CCI snow products to improve the modelling of snow dynamics in ORCHIDEE. In our model, the snow processes are represented with a physically-based approach where the main processes driving the temporal evolution of the snowpack such as ageing, compaction, sublimation, melting and refreezing, are represented with a 1D-physical system neglecting the lateral transfers.

In the original version of the model (Wang et al., 2013), the snowpack was vertically discretized in 3 layers for which snow temperature, density and liquid water content are prognostic variables. However, Charbit et al., (2024) have shown that replacing the 3-layer discretisation with a 12-layer one, following Decharme et al. (2016) improved the representation of the snow dynamics and especially snow temperature over glacier surfaces. For the sake of code consistency and after various tests, a vertical discretisation of the snowpack into 12 layers is now used in ORCHIDEE v4.3 for all surfaces.

Snow is uniformly distributed over the grid cell regardless of vegetation distribution, and the snow cover fraction (SCF) ranges between 0 and 1 according to the snow amount. SCF is parameterised following the formulation of Niu and Yang (2007) which has been shown to better represent the seasonal variation of the relationship linking snow mass (product of snow density and snow depth) and SCF thanks to its dependence on snow density:

$$SCF = \tanh\left(\frac{d_{snow}}{2.5 z_{0,bare} \times \left(\frac{\langle\rho_{snow}\rangle}{\rho_{min}}\right)^{m}}\right) \quad (1)$$

where ρ_{snow} is the snow density averaged over the total thickness of the snowpack (d_{snow}), ρ_{min} is the minimum value of snow density (set to 50 kg m^{-3}), $z_{0,bare}$ is the snow-free ground roughness length (set to 0.01 m) and *m* (set to 1.0 in ORCHIDEE) is an adjustable parameter.

The energy balance at the snow-atmosphere interface is solved at the model time step (30 mn), mostly driven by the snow albedo, which is a key parameter in the model, dependent on snow age and temperature.

Compared to the earlier version presented by Wang et al. (2013), the albedo scheme has been modified and snow albedo is computed for each PFT and each spectral band *b* (visible or near-infrared (NIR) albedo) following the formulation of Chalita and Le Treut (1994):

$$\alpha_{snow,PFT,b} = \alpha_{aged,PFT,b} + \alpha_{dec,PFT,b} exp\left(-\frac{t_{agesnow}}{\tau_{snow}}\right) \quad (2)$$

where $\alpha_{aged,PFT,b}$ represents the albedo of a snow-covered surface after snow aging (old snow) and $\alpha_{dec,PFT,b}$ is defined so that its sum with $\alpha_{aged,PFT,b}$ represents the albedo of fresh snow (i.e., maximum snow albedo). τ_{snow} is the time constant of the albedo decay and $t_{agesnow}$ is the snow age and is parameterised as follows:

$$t_{agesnow}(t+dt) = \left[\, t_{agesnow}(t) + \left(1 - \frac{t_{agesnow}}{\tau_{max}}\right) \times dt\right] \times exp\left(-\frac{P_{snow}}{\delta_c}\right) + f_{age} \qquad (3)$$

where τ_{max} is the maximum snow age, P_{snow} is the amount of snowfall during the time interval dt and δ_c is the critical value of solid precipitation necessary for reducing the snow age by a factor 1/e. In addition, low surface air temperatures found in arctic regions slow down the metamorphism and therefore the snow aging. This effect can be accounted for with the function f_{age} expressed as:

$$f_{age} = \left[\frac{\left(t_{agesnow}(t) + \left(1 - \frac{t_{agesnow}}{\tau_{max}}\right) \times dt\right) \times exp\left(-\frac{P_{snow}}{\delta_c}\right) - t_{agesnow}(t)}{1 + g_{temp}(T_{surf})}\right] \qquad (4)$$

With

$$g_{temp}(T_{surf}) = \left[\frac{max(T_0 - T_{surf},\ 0)}{\omega_1}\right]^{\omega_2} \qquad (5)$$

Where ω_1 and ω_2 are tuning constants, calibrated to 7 and 4 respectively over Greenland by Charbit et al. (2024). This last feature is just applied to glaciers in the default version of ORCHIDEE, but could be of interest with snow on vegetation.

The albedo is computed separately for the visible and near-infrared spectral bands. However, to compute the upward shortwave radiation, an arithmetic mean between the visible and the near-infrared albedo is considered.

2.3 ORCHIDEE v4.3 – Surface albedo computation

In ORCHIDEE v4.3, the radiative transfer scheme used to calculate the surface albedo (McGrath et al. (2016)), was updated following Ardaneh et al. (2025). The radiative transfer within vegetation canopies is represented using a multi-layer two-stream radiative transfer model. This scheme accounts for absorption and scattering processes within the canopy by solving coupled equations for upward and downward radiative fluxes. For vegetated areas, the albedo is computed as a combination of leaf and background (bare soil) contributions.

In the presence of snow, the albedo is computed differently whether the PFT corresponds to a low vegetation (bare soil and grasslands), or a forest.

For low vegetations (LV), it is assumed that snow covers the vegetation, and the computation of the resulting albedo for that PFT is equal to a weighted average of the snow albedo and the vegetation albedo directly (the weights being the snow cover fraction, calculated as presented in equation (1)):

$$\alpha_{LV,PFT,b} = \alpha_{snow,PFT,b} \times SCF + (1 - SCF)\alpha_{veget,PFT,b} \qquad (6)$$

However, for forest PFT, it is assumed that there is no snow on the canopy and that snow is under the trees, on the ground. Therefore, snow only contributes to the background albedo. The background albedo is also calculated as a weighted mean between the grid cell background albedo and the snow albedo:

$$\alpha_{bg,forest\ PFT,b} = \alpha_{snow,PFT,b} \times SCF + (1 - SCF)\alpha_{bg,PFT,b} \tag{7}$$

Then, to retrieve the total albedo of the PFT, this background albedo is used as an input (among many other inputs depending on the vegetation type) in the radiative transfer scheme and the resulting albedo is computed.

$$\alpha_{forest\ PFT,b} = f(\alpha_{bg,forest\ PFT,b}, \dots) \tag{8}$$

2.4 New model developments – snow albedo and snow cover fraction parameterisation

Previous studies have demonstrated the influence of vegetation on snow cover and surface albedo (Niu and Yang, 2004, Broxton et al., 2015). Several mechanisms may explain these effects. The presence of trees limits the amount of snow that can accumulate on the ground; leaves and other vegetative debris may be deposited on the snow surface, thereby altering its albedo; and surface roughness varies with vegetation type, implying that different snow depths are required for complete ground coverage.

In the current version of the model, some of these processes are represented. For instance, snow albedo parameters depend on the plant functional type (PFT) on which the snow lies. However, several effects remain unaccounted for. In particular, snow cover is presently calculated using an average surface roughness per pixel and is evaluated at the grid-cell level, without explicitly considering the characteristics of individual PFTs. Moreover, the snow cover fraction is assumed to be identical for all PFTs within a given grid cell, whereas in reality, different vegetation types are unlikely to exhibit the same degree of snow coverage. This simplification may lead to significant biases in the estimation of albedo.

The objective of this study is therefore to address these limitations by revising the parameterisation of snow cover as a function of vegetation, as well as the representation of snow–albedo interactions within the ORCHIDEE model. The main equations used to compute the snow cover fraction (SCF) and albedo are accordingly modified to account for vegetation effects.

To better represent the impact of vegetation on the SCF, this variable is now calculated separately for each PFT instead of estimating a mean SCF for the entire pixel. Equation (1) becomes equation (9). A new set of parameters $f_{scale,PFT}$ is introduced to account for the diversity of the different PFT. $f_{scale,PFT}$ corresponds to a scaling factor and physically represents the impact of the vegetation's roughness on the SCF. Although fresh snow density can be as low as 20 kg/m3 in some specific conditions, it is in most cases above 100 kg/m^3. The term ρ_{fresh}, corresponding to a median fresh snow density, is set to 100 kg/m^3, which is more realistic than the ρ_{min} value from equation (1) (Pomeroy et al., 2001). The other terms do not change. This SCF is assumed to be the snow cover fraction on the ground, as opposed to the snow cover fraction on top of the canopy.

$$SCF_{PFT} = tanh\left(\frac{d_{snow}}{f_{scale,PFT}\, z_{0,bare}\frac{\langle\rho_{snow}\rangle}{\rho_{fresh}}}\right) \quad (9)$$

Now that the SCF is calculated per PFT, the albedo for each spectral band b is calculated as a weighted average of the snow free albedo $\alpha_{snowfree}$, and the PFT-wise snow cover albedo ($\alpha_{snow,PFT,b}$), the weights being the proportion of PFT $f_{veg,PFT}$ multiplied by its corresponding SCF (SCF_{PFT}). Equation (10) replaces equations (7) and (8). Here, $\alpha_{snowfree,b}$ is either the vegetation albedo (for bare soil and low vegetations), or the background albedo (for forests).

$$\alpha_b = (1 - SCF_{tot})\alpha_{snowfree,b} + \sum_{PFT} f_{veg,PFT}\, SCF_{PFT}\alpha_{snow,PFT,b} \quad (10)$$

In turn, equation (2) is slightly modified, and becomes equation (11). The term α_{dec} is replaced by $\alpha_{max} - \alpha_{aged}$ in order to directly use a maximum albedo value, which is easier to understand. The time constant τ_{snow} becomes PFT-dependant ($\tau_{snow,PFT}$), as the vegetation can impact the snow aging differently.

$$\alpha_{snow,PFT,b} = \alpha_{aged,PFT,b} + \left(\alpha_{max,PFT,b} - \alpha_{aged,PFT,b}\right)\exp\left(-\frac{t_{agesnow}}{\tau_{snow,PFT}}\right) \quad (11)$$

For bare soil and low vegetation types, since the snow is deposited above the vegetation, we consider that the maximum albedo $\alpha_{max,PFT,b}$ is the same for all the PFT, and should be equal to the albedo of fresh snow.

3. Data

Several technical challenges arise when attempting to determine the most appropriate parameter values for each PFT. Model evaluation relies on multiple satellite-derived datasets, including CCI Snow SCFG, snow water equivalent (SWE), MODIS albedo, and PFT maps derived from CCI Land Cover (CCI LC). These are complemented by two additional datasets: the IPCC AR6 WG I regional classification (Gutierrez et al., 2021) and a slope map used within ORCHIDEE.

3.1 Presentation of the CCI Snow products

	SCFG	**SCFV**	**SWE**
Product name	Snow Cover Fraction Ground (from MODIS)	Snow Cover Fraction Viewable (from MODIS)	Snow Water Equivalent
Version	V4.0	V4.0	V4.0
DOI	doi:10.5285/375ffdb8f0a445e380b4b9548655f5f9	doi:10.5285/bc13bb02a958449aac139853c4638f32	doi:10.5285/edf8abd23f4a40aabd4d52e48dec06ea
Description	Daily snow cover fraction (0-100%) **on the ground** per pixel for global land areas (excluding pixels containing permanent snow and ice, water and salt lakes)	Daily snow cover fraction (0-100%) **on top of the forest canopy** per pixel for global land areas (excluding pixels containing permanent snow and ice, water and salt lakes)	Daily snow water equivalent (in mm) per pixel, representing the amount of water stored in the snowpack Covers the Northern Hemisphere land areas, excluding mountainous regions, glaciers, and Greenland
Cloud handling	Clouds are masked		Not affected by clouds
Data Source	Medium-resolution optical satellite data		Passive microwave satellite data (brightness temperatures) combined with in-situ snow depth measurements
Instrument	MODIS		SMMR, SSM/I and SSMIS PMR (merged product)
Spatial resolution	~1 km per pixel for MODIS		0.10-degree latitude-longitude grid
Uncertainty	Estimate of Unbiased Root Mean Square Error (RMSE) per pixel		Statistical standard deviation on each pixel
Auxiliary datasets	- **ESA CCI Land Cover 2000**: Masks water bodies and permanent snow/ice (aggregated to the pixel size of SCF product) - Salt lake mask generated by ENVEO - **Forest Canopy Transmissivity Map**: Derived from ESA CCI Land Cover 2000 and Landsat tree cover density map (Hansen et al., 2013, DOI: 10.1126/science.1244693) for canopy correction	- **ESA CCI Land Cover 2000**: Masks water bodies and permanent snow/ice (aggregated to the pixel size of SCF product) - Salt lake mask generated by ENVEO	- **ESA CCI Land Cover 2000**: Masks water bodies (aggregated to the pixel size of SWE product) - **ETOPO5-based Mountain Mask**: Used to exclude mountainous regions in the Northern Hemisphere (developed for the ESA GlobSnow project)
Other information	Forest canopy correction is applied based on the forest canopy transmissivity map		

Table 2: Snow CCI products description

The Snow CCI products (Solberg et al., 2021) provide several global daily time series of essential climate variables (ECV) related to snow:

- Snow Cover Fraction Viewable (SCFV)
- Snow Cover Fraction Ground (SCFG)
- Snow Water Equivalent (SWE)

The SCFV corresponds to snow on top of open areas and vegetation like forest canopies, while the SCFG is the snow on the ground for open land, corrected for masking by trees in forested areas. The snow cover for each grid cell is given as a percentage. The SWE indicates the amount of snow accumulated on land surfaces, as an equivalent height of water.

In this task, we worked with the CCI Snow V4.0 products (Barella et al., 2025). More details on the products are provided in Table 2.

3.2 Presentation of the other products: albedo and PFT maps

The MODIS daily global albedo product (doi:10.5067/MODIS/MCD43C3.061) is also used in this analysis, since SCF and albedo are interrelated. The MODIS Albedo products MCD43A3 available at a resolution of 0.05° and over the period 2000-2020 was chosen to evaluate the model predictions, analyse model errors and calibrate the model parameters.

In order to describe the vegetation, we used the PFT maps derived from the ESA CCI MRLC project (PFT V3.0 product, Harper et al., 2023).

4. Methodology

4.1 Multi-site parameter optimisation

The methodology is structured in two main steps. First, the ORCHIDEE model is modified to introduce vegetation-dependent parameterisations of snow albedo and SCF, as presented in section 2.3. Secondly, the parameters associated with these new formulations are calibrated using a site-based approach.

A global optimisation was deemed impractical due to computational constraints and the difficulty of interpreting results over heterogeneous grid cells, where multiple PFTs coexist and error compensation may occur. Instead, calibration is performed at carefully selected sites representative of individual PFTs, allowing a more controlled analysis of the processes involved.

For calibration, the data assimilation tool associated to ORCHIDEE (ORCHIDAS) is used (Bastrikov et al., 2018).

4.1.1 Site selection procedure

Constraints

The selection of calibration sites aims to balance three main constraints: (i) maximising the availability of satellite observations, (ii) ensuring a dominant vegetation type, and (iii) maintaining representativeness across different climatic regions.

To this end, sites were selected for each PFT based on:

- a high number of valid SCF observations over the 2011–2016 period, with SCF values exceeding 10%;
- a dominant PFT fraction within the grid cell;
- minimal temporal variability in vegetation cover over the study period;
- low topographic influence, enforced by excluding grid cells with slopes greater than 2%.

In addition, the spatial distribution of sites is constrained using the AR6 regional classification. The number of selected sites per region is made proportional to the regional occurrence of each PFT, ensuring that the resulting parameter values are representative of global conditions.

Selection metric: desirability function

To quantify the suitability of each grid cell for calibration, a selection metric (hereafter referred to as the desirability function) is defined. It is based on the concept of acquisition functions used in Bayesian optimization, which aims to estimate the potential gain in information by exploring a spatial domain. The idea is to assign a score ranging from 0 to 1, to each point of this domain and then select those with the highest scores.

Let $n_{snow}(x)$ denote the number of valid SCF observations at grid cell x, n_{days} the total number of days and $f_{veg,PFT}(x)$ the fraction of the dominant PFT in that grid cell. The desirability function $V(x)$ is defined as:

$$V(x) = \frac{n_{snow}(x)}{n_{days}} \times f_{veg,PFT}(x) \tag{12}$$

This metric favours grid cells that both exhibit frequent snow conditions and are dominated by a single vegetation type. To avoid selecting sites with too low values, a threshold of 0.1 is set. It means that, for a homogeneous pixel with a PFT fraction equal to 100%, we need to have at least 10% of the total period with SCF observations. This may seem low, but the summer months tend to be excluded with no snow, and SCF observations tend to be scarce.

Selection algorithm

All datasets (SCF, PFT, regions, slope) are first regridded onto a common 0.05° grid. Masks are applied to exclude:

- regions with slopes greater than 2%;
- grid cells without a dominant PFT;
- grid cells where PFT fractions vary over time;
- Greenland and very high latitude regions (above 70°N) due to persistent data limitation.

For each PFT, and within each AR6 region in which sites have to be selected, we consider a set of N grid cells X= $\{X_1, X_2, \ldots, X_N\}$, with a desirability function value above the threshold of 0.1, and belonging to the region. Each point X_i is defined by its coordinates (lat_i, lon_i) and its desirability function value v_i.

The first selected point x^* is the one with the highest desirability function value such that $x^* = \arg\max_{x_i \epsilon X} v_i$.
We initialize the set of selected points $S = \{x^*\}$.

Then, we select iteratively the most distant points. At each iteration, we select the point x_{new} that is the farthest from the set of already selected points. Distance is measured using the Manhattan distance:

$$d(x_i, x_j) = |lat_j - lat_i| + |lon_j - lon_i| \tag{13}$$

The next point is chosen by maximizing the minimum distance to the selected set:

$$x_{new} = \arg\max_{x \epsilon X \setminus S} \min_{q \epsilon S} d(x, q) \tag{14}$$

Once selected, this point is added to the set: $S \leftarrow S \cup \{x_{new}\}$
The process continues until all points have been selected, ensuring that each newly added point is as far as possible from the previously selected ones.

A total of 20 sites per PFT is selected following this procedure. The procedure is summarised in Figure 1.

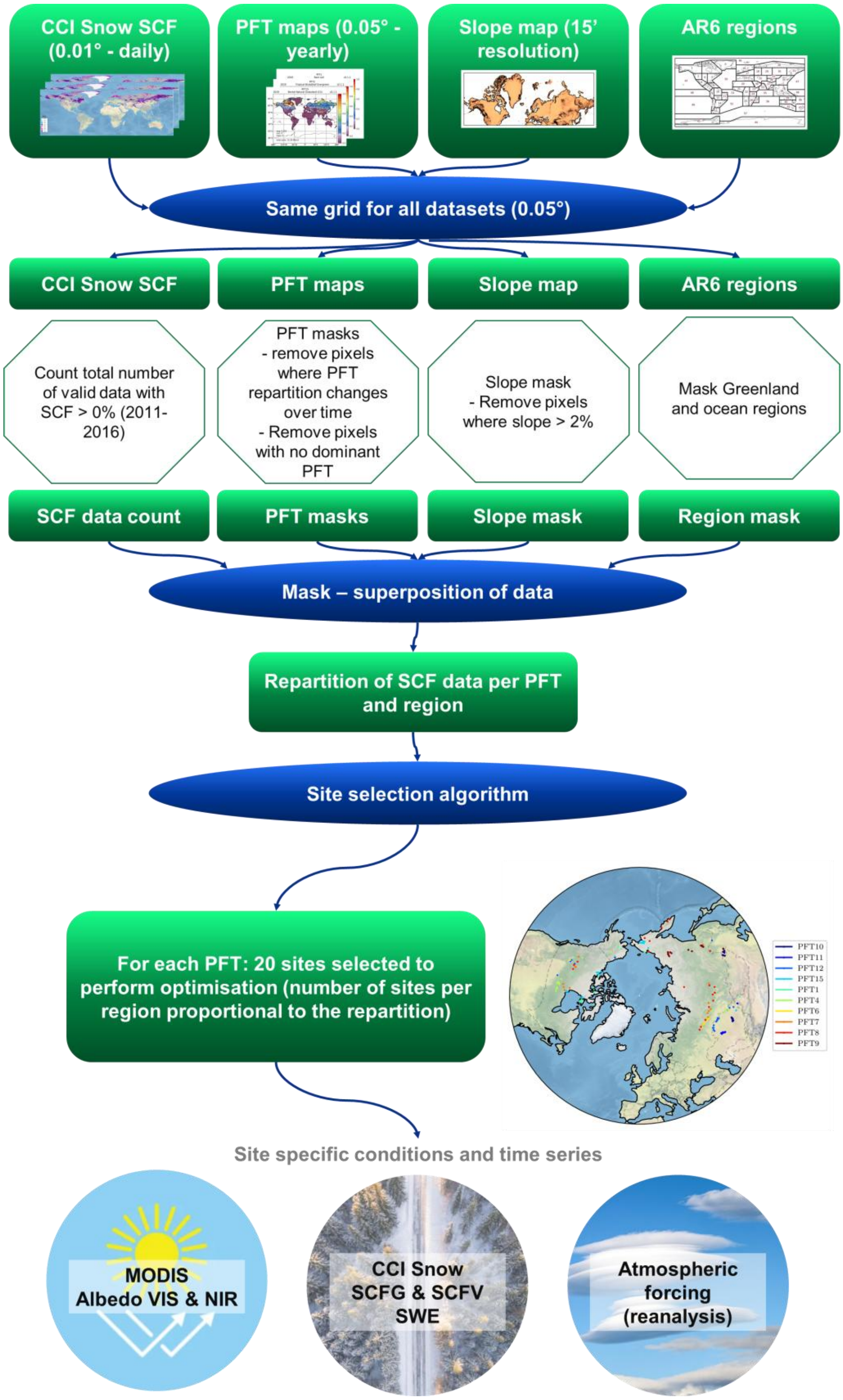

Figure 1: Site selection procedure

Study regions and PFT distribution

Figure 2 shows the geographical distribution of the study regions, all located north of 40°N. The regions are listed in Table 3. Depending on the plant functional type (PFT), one or several regions are represented.

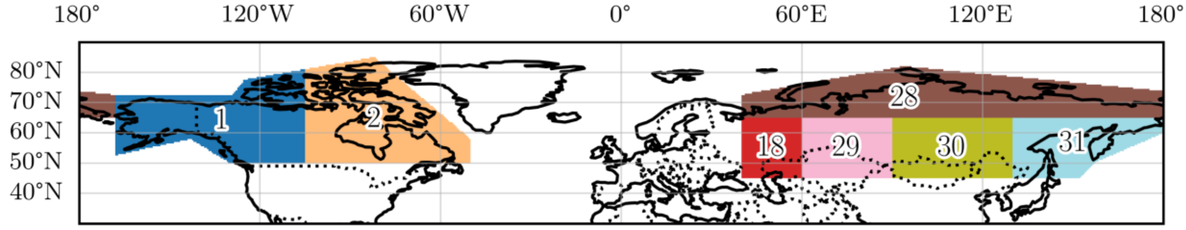

Figure 2: AR6 regions from which site are selected

REGION	1	2	18	28	29	30	31
NAME	N.W.North-America	N.E.North-America	E.Europe	Russian-Arctic	W.Siberia	E.Siberia	Russian-Far-East

Table 3: AR6 region names

Figure 3 presents the spatial distribution of the 15 PFTs. Some PFTs are widespread, while others are more localised (e.g. PFT9). PFT15 is particularly dominant and is present in almost all regions, highlighting the importance of accurately representing this vegetation type.

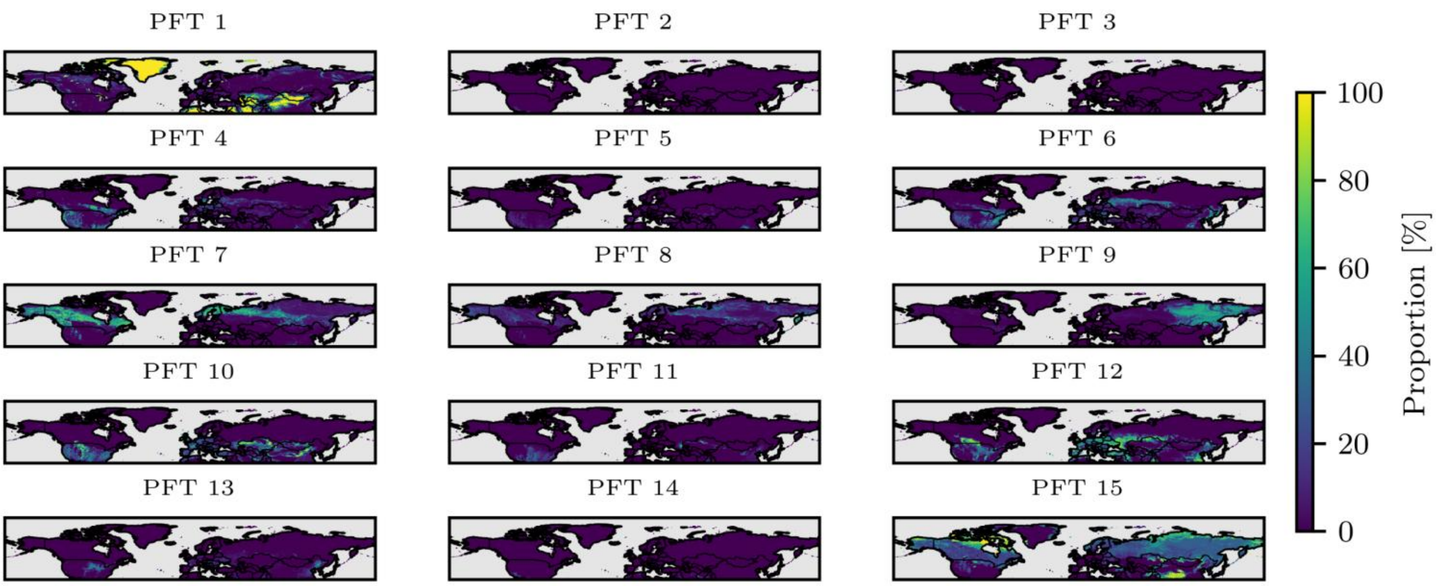

Figure 3: Repartition of the different PFT

4.1.2 Parameter calibration

Figure 4 summarises the parameter calibration process. More details are provided in the following paragraphs to describe the methodology.

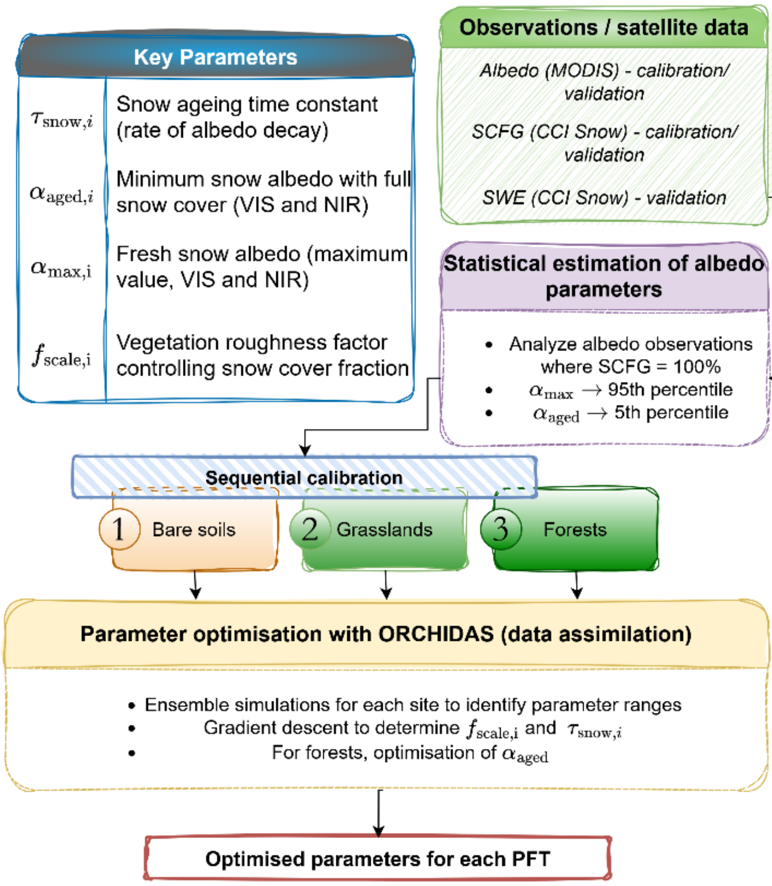

Figure 4: Parameter calibration process

Bare soils and low vegetation PFTs

For bare soil and grassland PFTs, the absence or the low height of a canopy considerably simplifies the analysis, as snow is directly exposed at the atmosphere interface and radiative interactions are not affected by vegetation structure. In this context, the parameterisation of snow albedo can be constrained using satellite observations under well-defined conditions.

The maximum snow albedo α_{max} is assumed to correspond to fresh snow and is prescribed as a constant value common to all bare soil and grassland PFTs (one value for VIS and one for NIR). A statistical analysis of observed albedo under fully snow-covered conditions (SCF = 100%) is nevertheless performed to ensure that this prescribed value remains consistent with satellite observations. In contrast, the minimum snow albedo under fully snow-covered conditions $\alpha_{aged,PFT}$ is directly estimated from observations for both VIS and NIR spectral bands. It is derived from the lower tail of the albedo distribution (5th percentile), representing aged snow conditions, while the upper tail (95th percentile) is used as a consistency check for α_{max}.

The remaining parameters, namely the snow ageing timescale $\tau_{snow,PFT}$ and the snow cover fraction parameter $f_{scale,PFT}$ are calibrated using an iterative ensemble-based approach. First, a broad range of parameter combinations is explored through ensemble simulations at each calibration site. The resulting simulations are compared against satellite observations of both SCF and albedo, allowing the identification of plausible regions of the parameter space. In a second step, the parameter space is progressively reduced by focusing on subsets of parameter combinations that provide the best agreement with observations. This iterative refinement enables the identification of robust parameter values while limiting the risk of error compensation between processes.

Finally, individual parameters are optimised sequentially by fixing one parameter to its most representative value and refining the other based on its impact on model performance. This strategy ensures that the calibrated parameters remain physically meaningful, minimise overlap between the processes they represent, and retain robustness with respect to potential future model developments.

Forested PFTs

The calibration over forested PFTs is more complex due to canopy-related effects (strongly depending on tree structure and leaf type) and radiative transfer processes. In particular, the observed surface albedo not only depends on snow on the ground but also on the presence of snow intercepted and retained on the canopy.

Analysis of the data reveals contrasting behaviours: low albedo values are generally associated with limited snow cover on vegetation (SCFV), while high albedo values correspond to conditions where the canopy is snow-covered. In the present study, a manual tuning approach is employed to adjust the background snow albedo parameters. Maximum albedo values are estimated by testing multiple combinations of VIS and NIR maximum albedo parameters. The parameter set that provides the best performance during mid-winter (when the snowpack is well developed) across the majority of sites is selected. This approach has some limitations as the maximum albedo parameters obtained may be different from the actual background snow albedo, as the observations correspond to the albedo above the canopy and snow on the canopy can affect the results. The minimum albedo (α_{aged}) is derived from snow-free conditions.

The snow aging parameter is then calibrated, followed by refinement of the SCF parameter.

Due to the complexity of canopy processes, the current approach does not explicitly represent snow interception and retention on vegetation. This limitation is addressed in the discussion.

4.2 Multi-site and global parameters validation

Once the optimised parameters are identified, POST simulations are run. First, they are run on all the calibration sites, with the full set of optimised parameters to see how the model behaves in these conditions, and are compared to a PRIOR simulation with the default model configuration. On sites, a rapid 6-year spinup is performed by looping over 2011-2016 once, and then, the results of the second loop are studied and compared with observations.

For the sites' configuration, the sites were optimised based on masked observations: only the observations with SCF above 10% and both available albedo and SCF data were used. The analysis of the results is then split into two parts: one analysing the results with the masked data, and in a second step, analysing the results from the whole time-series, without the mask, in order to validate the model more comprehensively.

To evaluate the new version, two pan-Arctic simulations are also run: a PRIOR and a POST simulation. Both simulations are run from 1992 to 2019, and only the years 2010-2019 are considered for evaluation.

5. Results

5.1 Optimised parameters for each PFT

The equations were slightly modified between the PRIOR and POST versions, but equivalent parameters can still be identified. In particular, the maximum albedo for the visible (VIS) and NIR wavelengths (α_{max}) in the PRIOR configuration corresponds to the sum of α_{aged} and α_{dec}. The parameter $f_{scale,PFT}$ can be inferred from the denominator terms of the SCF equation (cf. equations (1) and (9)). With the new parameterisation, reproducing PRIOR conditions would require $f_{scale,PFT} = 5$.
Table 4 summarises the parameter values for both configurations. The POST configuration corresponds to parameters derived from site-by-site optimisation.

	$\alpha_{aged,PFT,vis}$		$\alpha_{aged,PFT,nir}$		$\alpha_{max,PFT,vis}$		$\alpha_{max,PFT,nir}$		$f_{scale,PFT}$		$\tau_{snow,PFT}$	
PFT	PRIOR	POST	PRIOR	POST	PRIOR	POST	PRIOR	POST	PRIOR	POST	PRIOR	POST
1	0,68	0,75	0,615	0,47	0,98	0,95	0,665	0,65	5	0,01	15	13
2	0,24	0,04	0,37	0,13	0,38	0,205	0,47	0,295	5	5	15	5
3	0,07	0,04	0,08	0,13	0,15	0,205	0,24	0,295	5	5	15	5
4	0,5	0,04	0,5	0,13	0,8	0,205	0,8	0,295	5	5	15	5
5	0,5	0,04	0,5	0,13	0,8	0,205	0,8	0,295	5	5	15	5
6	0,5	0,04	0,32	0,13	0,8	0,14	0,502	0,23	5	5	15	5
7	0,5	0,04	0,491	0,13	0,8	0,305	0,638	0,395	5	5	15	5
8	0,5	0,04	0,5	0,13	0,8	0,205	0,744	0,295	5	5	15	5
9	0,45	0,04	0,314	0,13	0,589	0,305	0,324	0,395	5	5	15	5
10	0,68	0,7	0,626	0,51	0,98	0,95	0,676	0,65	5	0,1	15	16
11	0,68	0,74	0,626	0,49	0,98	0,95	0,676	0,65	5	0,65	15	13
12	0,68	0,68	0,626	0,48	0,98	0,95	0,676	0,65	5	3	15	7
13	0,68	0,68	0,626	0,48	0,98	0,95	0,676	0,65	5	3	15	7
14	0,68	0,75	0,626	0,47	0,98	0,95	0,676	0,65	5	0,1	15	18
15	0,68	0,75	0,626	0,47	0,98	0,95	0,676	0,65	5	0,1	15	18

Table 4:PRIOR and POST parameters

5.2 Site-level evaluation

5.2.1 Global RMSE analysis across PFTs

Figure 5 shows the distribution of albedo RMSE across sites for each PFT. PRIOR corresponds to the default ORCHIDEE configuration, while POST corresponds to the optimised configuration, compared to masked observations, as used in the calibration procedure. PRIOR_ALL and POST_ALL represent evaluations over the full time series without masking. Medians are shown as solid lines and means as dashed lines, with individual site values coloured by region. Equivalent results for SCF are shown in Figure 6.

For albedo, POST generally reduces RMSE across most PFTs. Both median and mean RMSE values are lower than in PRIOR, which was the primary objective. However, regional disparities remain. For example, for PFT8, PRIOR performs better in regions 31 and 28, whereas POST improves results in other regions but degrades performance in these two. Except for PFT9, maximum RMSE values are consistently lower in POST.

For SCF, results are more mixed. Significant improvements are observed for low vegetation types, whereas results for forests are more variable. This likely reflects difficulties in representing sub-canopy snow and uncertainties in the CCI SCFG observations as they are estimated through transmissivity maps, adding more uncertainty to the data. Despite this, POST generally improves SCFG relative to PRIOR.

When evaluated over the full dataset (PRIOR_ALL and POST_ALL), performance often degrades in the POST configuration compared to the optimisation subset. For albedo, forested regions generally retain improved performances, but degradation is observed for PFT8 and PFT9 depending on the region. For low vegetation PFTs 10, 11 and 15, the RMSE range decreases but mean values often remain higher than in PRIOR_ALL.

A similar degradation is observed for SCF when considering the full dataset.

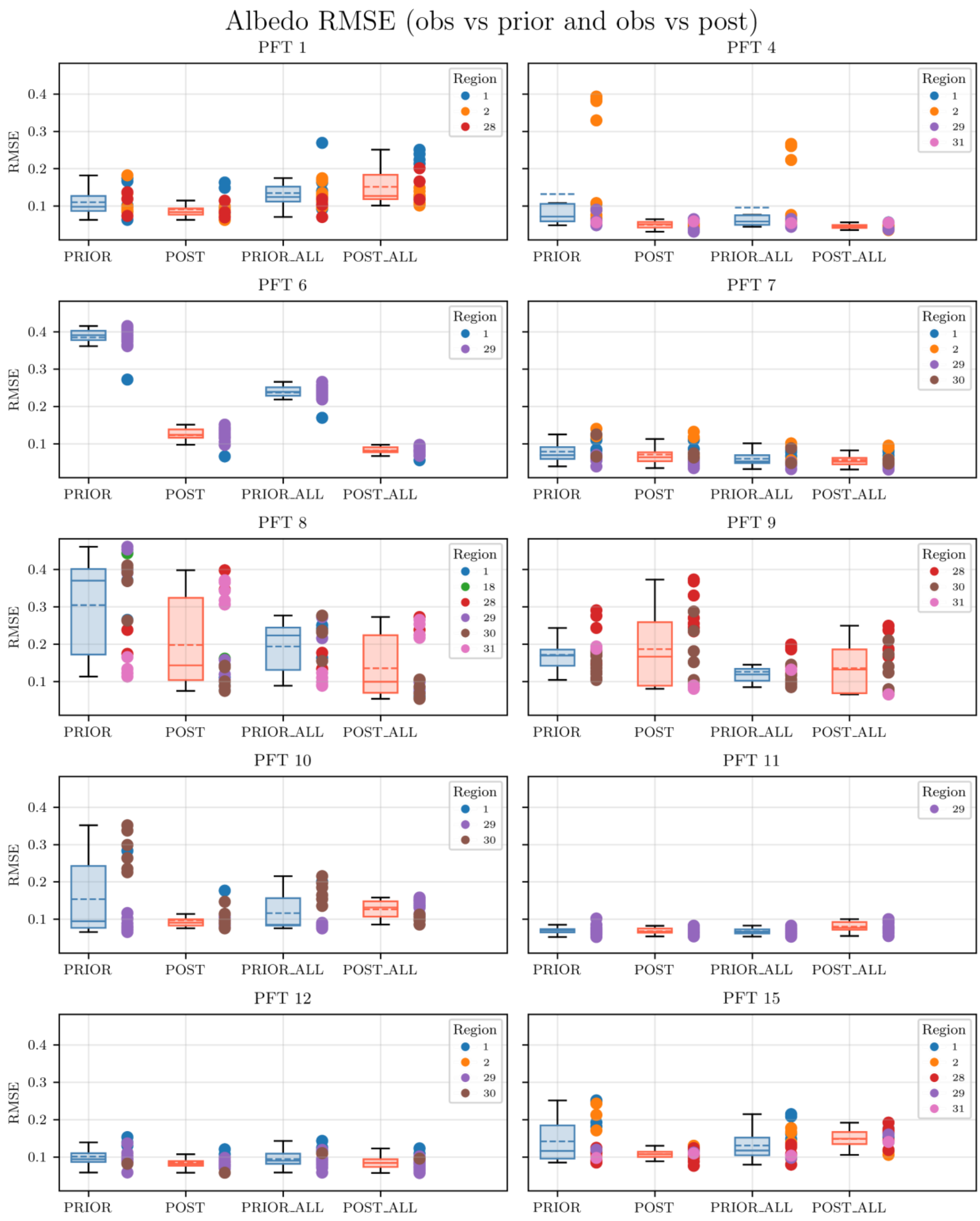

Figure 5: Albedo RMSE distribution across PFTs and sites

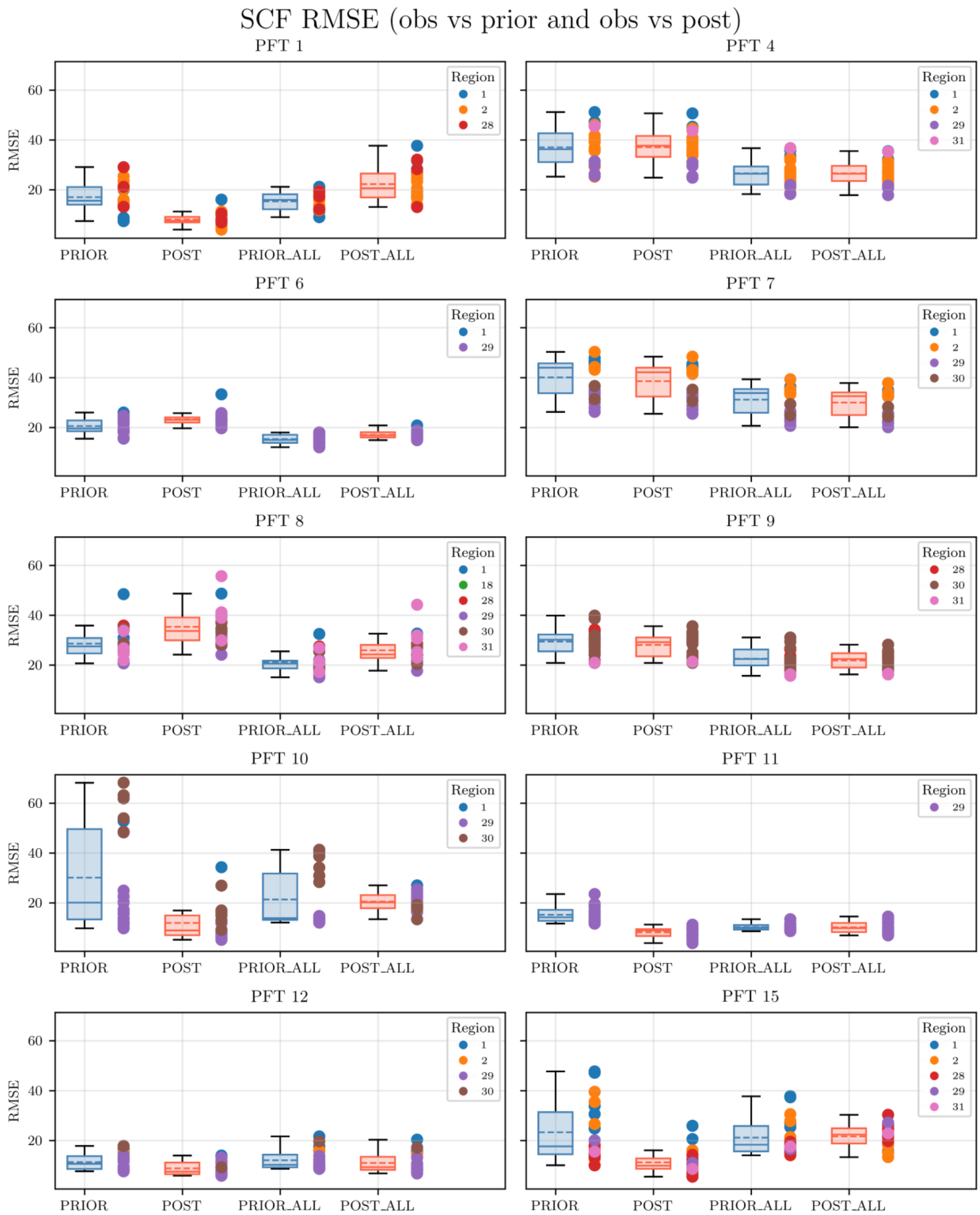

Figure 6: SCF RMSE distribution across PFTs and sites

5.2.2 Seasonal cycle analysis

Figures 7 and 8 show the monthly evolution of RMSE and bias for albedo and SCF, respectively. RMSE increases during winter due to the influence of snow, with peaks during accumulation and ablation periods.

POST reduces RMSE and bias during mid-winter (December–February) for most PFTs, especially tree PFTs for which large reduction errors are observed (e.g. for PFTs 4, 6 and 8). However, errors remain large during transition periods (early accumulation and melt) for grassland and crops PFTs. For forest PFTs, POST improves results except for PFT9, whereas for low vegetation, POST generally performs worse than PRIOR.

For low vegetations (PFT1, and 10-15), POST introduces a systematic positive bias in albedo, especially during transition periods. Conversely, PRIOR is more centred. For forests, POST tends to reduce the positive bias observed with PRIOR. For SCF, POST tends to overestimate snow cover over low vegetation and underestimate it for forests, whereas PRIOR generally underestimates SCF.

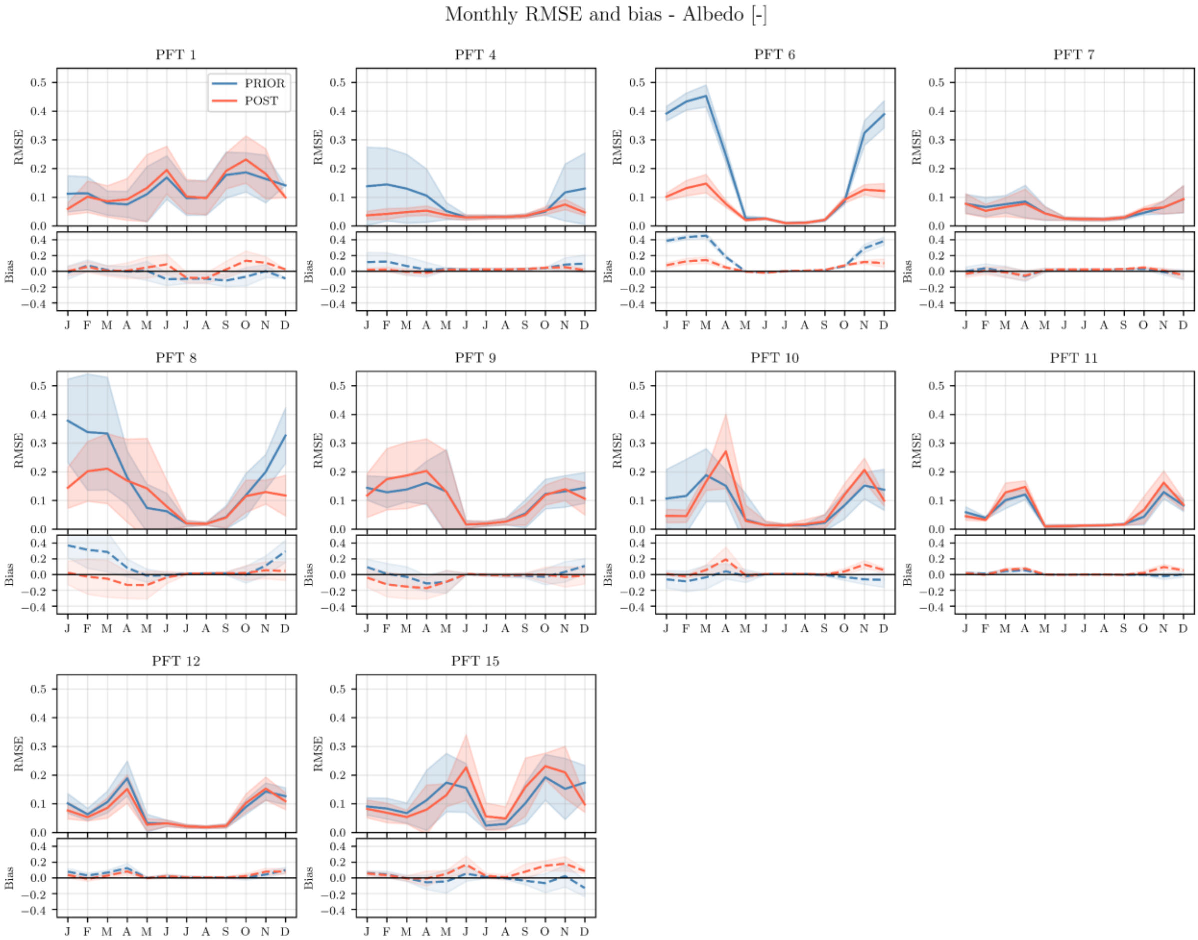

Figure 7: Monthly RMSE and bias on albedo per PFT

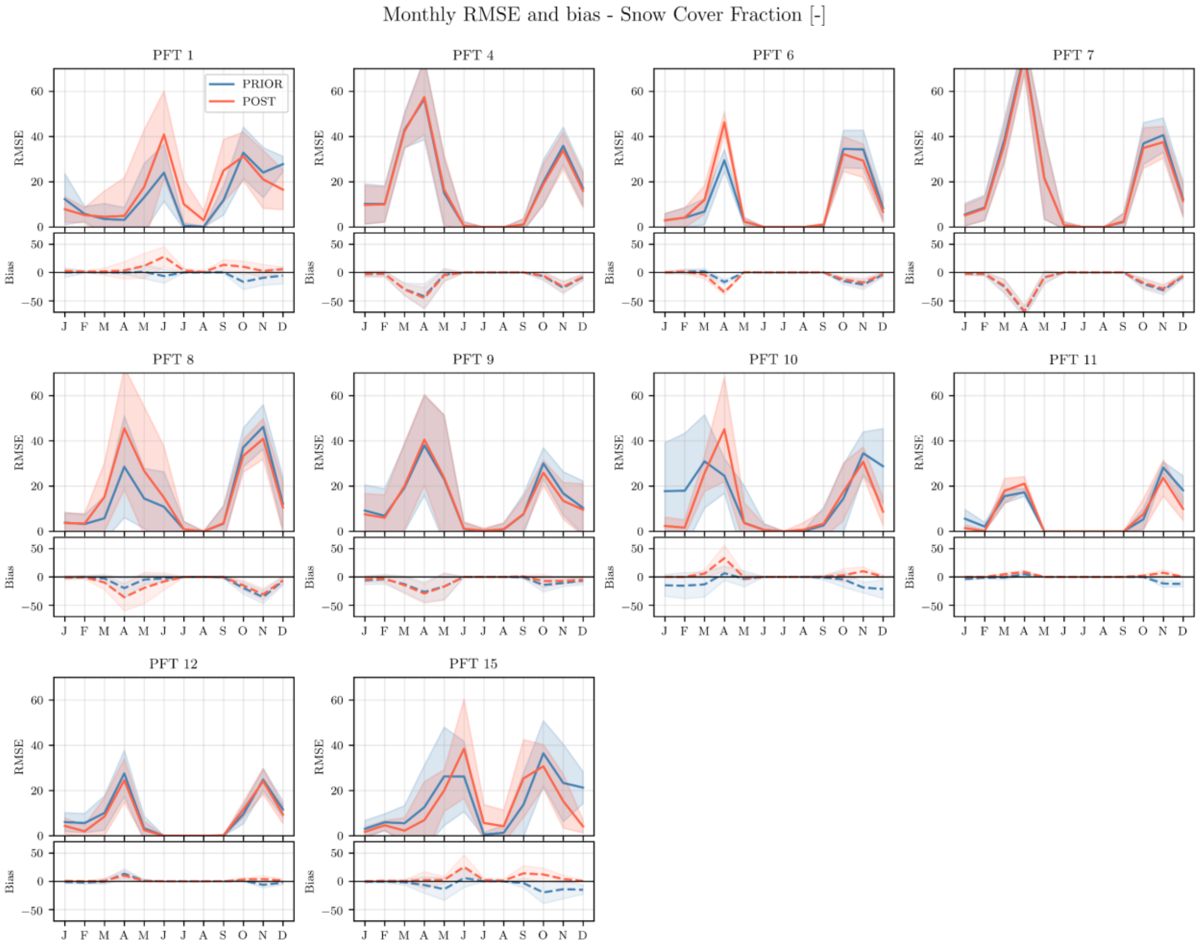

Figure 8: Monthly RMSE and bias on SCFG per PFT

Figures 9 and 10 illustrate seasonal cycles and biases for selected PFTs (PFT15 and PFT8). Results for other PFTs are provided in the appendix.

For low vegetations (e.g. PFT15), biases in albedo and SCF occur during similar periods, confirming their strong coupling. SCF largely controls albedo: overestimation of SCF leads to overestimation of albedo (POST), while underestimation leads to lower albedo (PRIOR). For North-America (regions 1 and 2), POST shows some improvements compared to PRIOR. However, for the other regions, POST biases are generally larger.

For forests, a strong inter-regional variability is observed, particularly for PFT8 (figure 10), with maximum albedo values ranging from 0.3 to above 0.7. This highlights the difficulty of defining a single parameter set for a given PFT across different regions presenting different regional climates and landscapes. For PFT8, SCF is underestimated in both configurations, and albedo biases dominate. POST produces intermediate albedo values compared to PRIOR, with regional variations.

Finally, snow water equivalent (SWE) shows limited differences between configurations, although feedbacks exist: lower albedo reduces SWE, which can further reduce SCF and thus albedo.

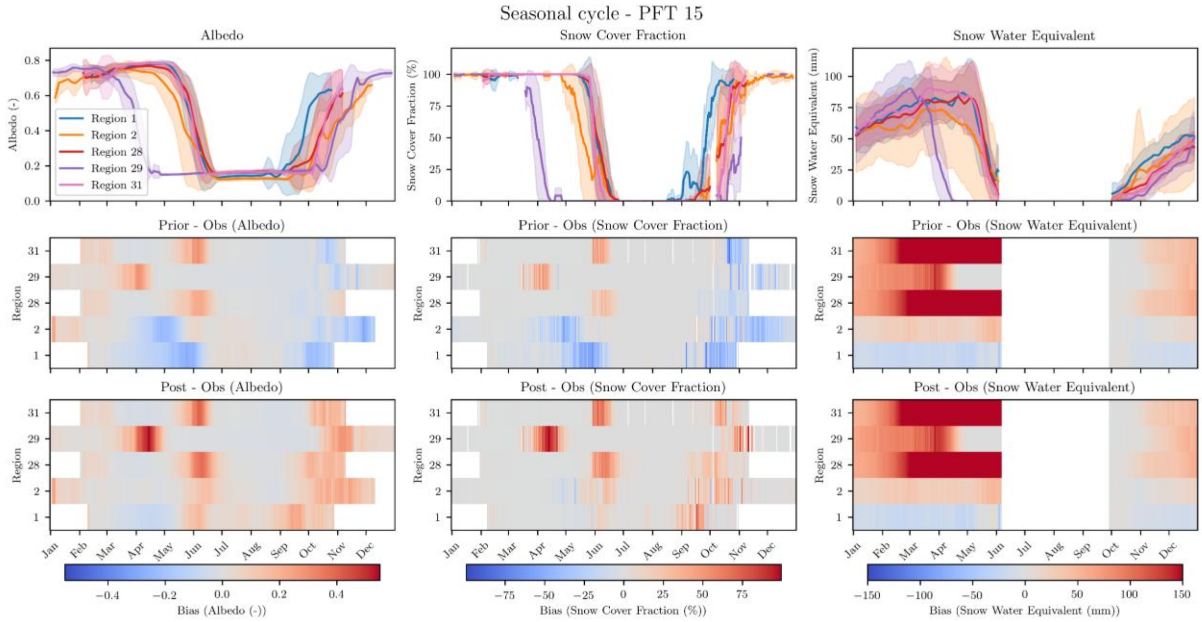

Figure 9: Seasonal cycle for PFT15 sites - albedo, SCFG, SWE - observations above, prior vs obs bias in the middle and post vs obs bias below

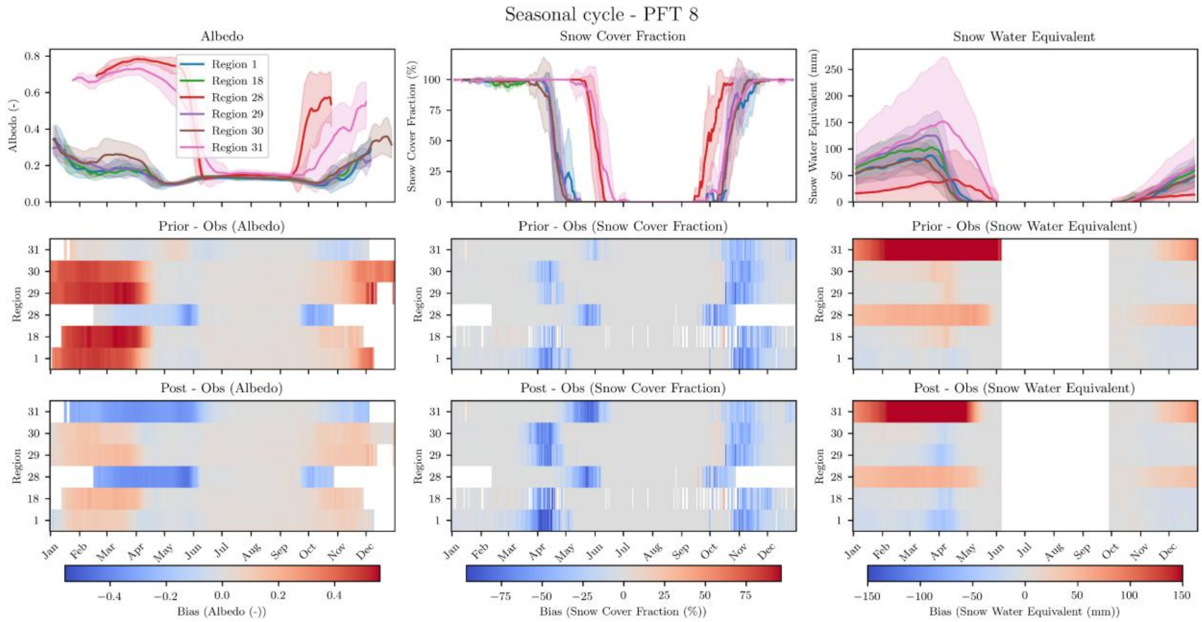

Figure 10: Seasonal cycle for PFT8 sites - albedo, SCFG, SWE - observations above, prior vs obs bias in the middle and post vs obs bias below

5.3 Global evaluation

Two pan-Arctic simulations (30–90°N) were conducted for 1992–2019, with analysis over 2010–2019.

Figure 11 shows winter RMSE for SWE (November–April) simulated with the PRIOR parameterisation. Errors are generally low south of 60°N, except in eastern Canada, and higher in northern Siberia. Figure 12 shows corresponding biases, with slight overestimation in northern regions and underestimation further south.
Results for PRIOR and POST are very similar for SWE, which is why only the figures from the PRIOR simulations are shown.

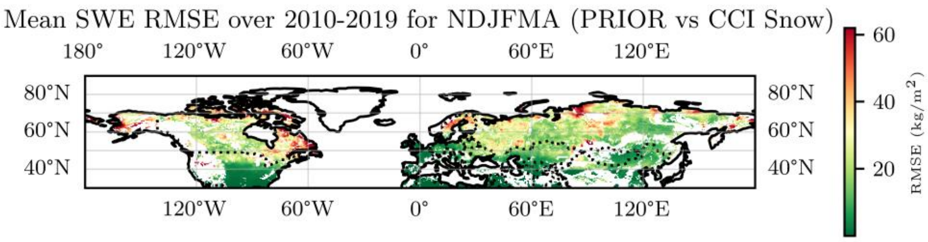

Figure 11: Pan-Arctic SWE RMSE between PRIOR and OBS averaged over 2010-2019 for snow season (from November to April)

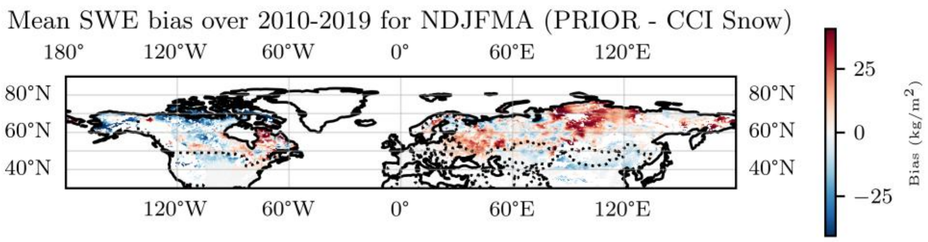

Figure 12: Pan-Arctic SWE bias between PRIOR and OBS averaged over 2010-2019 for snow season (from November to April)

Figures 13 and 14 show monthly albedo biases. POST exhibits stronger biases than PRIOR, with overestimation in regions dominated by PFT1 and PFT15 and underestimation in boreal forest regions (PFT7–9), consistent with site-level analysis.

Parameter analysis (Table 4) indicates that POST reduces maximum albedo values for low vegetation but still overestimates albedo due to SCF overestimation. For forests, lower maximum albedo values and shorter time constants likely contribute to underestimation.
Overall, site-level results are consistent with large-scale simulations, suggesting that the selected sites are broadly representative.

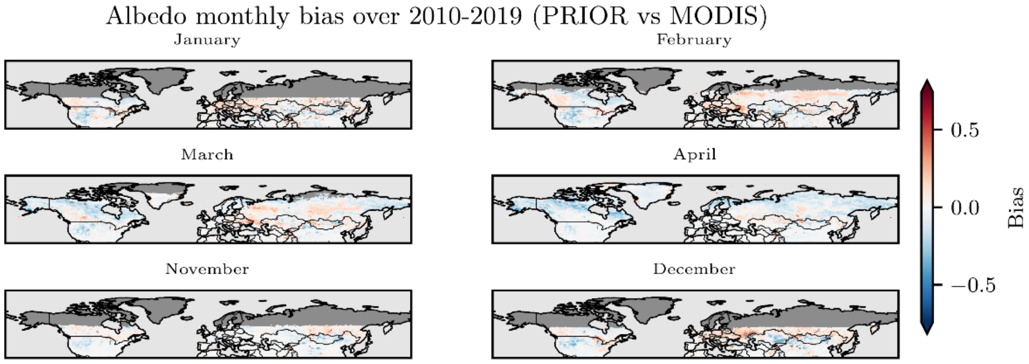

Figure 13: Pan-Arctic albedo monthly biases between PRIOR and obs (over 2010-2019)

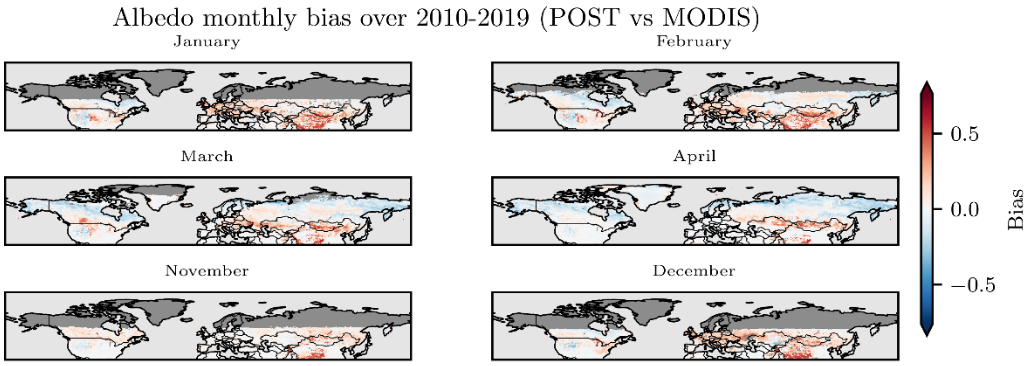

Figure 14: Pan-Arctic albedo monthly biases between POST and obs (over 2010-2019)

6. Discussion

6.1 Role of snow cover fraction and transition periods

The results show that POST performs better than PRIOR during mid-winter when SCFG is close to 100%, but struggles during accumulation and ablation periods. This reflects the optimisation strategy, which is dominated by conditions with high SCF, where sensitivity to parameters such as $f_{scale,PFT}$ is limited.

Transition periods are under-represented in the calibration dataset, leading to poor constraint of parameters controlling partial snow cover. Improving model performance therefore requires focusing calibration on these key periods.

Future optimisation should prioritise accumulation and melt phases, potentially using albedo as the primary constraint when SCF observations are sparse. The development of gap-filled SCF products (as planned by the Snow CCI team) could significantly improve this analysis.

6.2 Influence of vegetation on snow processes

Vegetation strongly controls both snow cover and albedo. Low vegetation exhibits relatively consistent behaviour, with albedo largely driven by snow properties and SCF. In contrast, forests show greater variability due to canopy structure, interception, and radiative effects.
For low vegetation, accurate representation of SCF is critical, as it directly controls albedo. In forests, albedo parameters themselves play a more dominant role, while SCF has a weaker influence.

6.3 Limitations in forest representation

The representation of snow in forested areas remains a major limitation. The current albedo model considers that snow covers only the ground, whereas canopy snow can be present part of the time and significantly increase albedo, even if it can fall or melt rapidly after snowfall. Our study demonstrates that this representation leads to systematic underestimation of albedo under high canopy snow conditions.
Two approaches could address this limitation:

- Explicit representation of canopy snow through modifications to the radiative transfer scheme, though this would require substantial development;
- An empirical correction to account for increased albedo under conditions favourable to snow interception.

6.4 Robustness of the calibration strategy

The site-based calibration approach provides a controlled framework and enables detailed analysis of vegetation-dependent processes. However, it relies on assumptions regarding site representativeness and observational data quality.

SCF products derived from optical remote sensing are affected by cloud cover and retrieval uncertainties. In forested areas, additional modelling assumptions further increase uncertainty, complicating our evaluation.

6.5 Consistency across scales and model sensitivity

The consistency between site-level and pan-Arctic results is encouraging, indicating that the selected sites capture key processes. Additionally, the limited impact of parameter changes on SWE suggests that snow–albedo feedbacks remain stable, allowing parameter tuning without major side effects on snow mass.

7. Conclusion and perspectives

This study highlights the complex interactions between snow processes, vegetation, and surface albedo, and demonstrates the challenges associated with their representation in land surface models such as ORCHIDEE.

The optimisation strategy significantly improves model performances during mid-winter conditions, when snow cover is close to 100%. However, it remains insufficient during key transition periods, such as snow accumulation and melting, which are critical for accurately capturing snow cover dynamics. These limitations primarily arise from the under-representation of partial snow cover conditions in the calibration datasets.

The results confirm the dominant role of vegetation in modulating snow–albedo interactions. Low vegetation PFTs are strongly controlled by snow cover fraction, whereas forested areas exhibit more complex behaviour driven by canopy structure, snow interception, and radiative transfer processes.

Despite these limitations, the consistency between site-scale and pan-Arctic simulations indicates that the calibration framework captures the main physical processes. Furthermore, the limited impact of parameter changes on snow water equivalent suggests that improvements can be pursued without destabilising the overall snow–albedo feedback.

Overall, this work provides a solid basis for future developments. Further work is needed to improve parameter estimation, particularly during transition periods. Key priorities include:

- Targeted calibration focusing on snow accumulation and melt phases;
- Improved use of albedo observations when SCF data are limited;
- Enhanced representation of snow–vegetation interactions, especially in forests;
- Development of canopy snow processes, either physically or empirically.

Despite the mixed performance of the POST configuration, the results remain coherent and physically interpretable. This provides a solid basis for further improvements, with strong potential for enhanced model performance through refined calibration strategies.

Special thanks

Two internships have been dedicated to the tasks of WP5.6. Some of the works presented here are direct results of these internships (Guillermo Cossio, summer 2023, and Benoît Lecomte, fall 2023, internal reports). Moreover, this project also benefited from the work of our LSCE colleagues (Vladislav Bastrikov, Luis Olivera, Simon Beylat and Vincent Tartaglione) on the optimisation of ORCHIDEE.

8. References

Alessandri, A., Catalano, F., De Felice, M., Van den Hurk, B., & Balsamo, G.: Varying snow and vegetation signatures of surface-albedo feedback on the Northern Hemisphere land warming. *Environmental Research Letters*, *16*(3), 034023, doi:10.1088/1748-9326/abd65f, 2021.

Barella, R., C. Mortimer, C. Marin, G. Schwaizer, M. Heinrich, T. Nagler, N. Mölg, S. Wunderle, X. Xiao, K. Luojus, P. Venäläinen, M. Takala, J. Pulliainen, J. Lemmetyinen, M. Moisander, and R. Solberg (2025) ESA CCI+ Snow ECV: Product User Guide, version 5.1, December 2025.

Bastrikov, V., Macbean, N., Bacour, C., Santaren, D., Kuppel, S. and Peylin, P.: Land surface model parameter optimisation using in situ flux data: Comparison of gradient-based versus random search algorithms (a case study using ORCHIDEE v1.9.5.2), *Geoscientific Model Development, 11(12),* 4739–4754, doi:10.5194/gmd-11-4739-2018, 2018.

Betts, A. K., Desjardins, R., Worth, D., Wang, S., and Li, J.: Coupling of winter climate transitions to snow and clouds over the Prairies, *Journal of Geophysical Research: Atmospheres, 119*, 1118–1139, doi:10.1002/2013JD021168, 2014.

Broxton, P. D., Harpold, A. A., Biederman, J. A., Troch, P. A., Molotch, N. P., and Brooks, P. D.: Quantifying the effects of vegetation structure on snow accumulation and ablation in mixed-conifer forests. *Ecohydrology, 8(6)*, 1073-1094, doi: 10.1002/eco.1565, 2015.

Chalita, S. and Le Treut, H.: The albedo of temperate and boreal forest and the Northern Hemisphere climate: a sensitivity experiment using the LMD GCM, *Climate Dynamics, 10*, 231-240, doi: 10.1007/BF00208990, 1994.

Charbit, S., Dumas, C., Maignan, F., Ottlé, C., Raoult, N., Fettweis, X., & Conesa, P.: Modelling snowpack on ice surfaces with the ORCHIDEE land surface model: application to the Greenland ice sheet. *The Cryosphere*, *18*(11), 5067-5099, 2024.

Decharme, B., Brun, E., Boone, A., Delire, C., Le Moigne, P. and Morin., S.: Impacts of snow and organic soils parameterization on northern Eurasian soil temperature profiles simulated by the ISBA land surface model, *The Cryosphere, 10*, 853-877, doi: 10.5194/tc-10-853-2016, 2016.

Forbes, T., Rossiter, D., & Van Wambeke, A.: *Guidelines for evaluating the adequacy of soil resource inventories* (Vol. 4). Cornell University, Department of Agronomy, 1987.

Gutiérrez, J.M., R. Ranasinghe, A.C. Ruane, R. Vautard, N. Arnell, E. Coppola, I. Pinto, D. Ruiz Carrascal, J. Sillmann, and C. Tebaldi, 2021: Annex VI: Climatic impact-driver and extreme indices. In *Climate Change 2021: The Physical Science Basis. Contribution of Working Group I to the Sixth Assessment Report of the Intergovernmental Panel on Climate Change*. V. Masson-Delmotte, P. Zhai, A. Pirani, S.L. Connors, C. Péan, S. Berger, N. Caud, Y. Chen, L. Goldfarb, M.I. Gomis, M. Huang, K. Leitzell, E. Lonnoy, J.B.R. Matthews, T.K. Maycock, T. Waterfield, O. Yelekçi, R. Yu, and B. Zhou, Eds., Cambridge University Press, pp. 2205-2214, doi:10.1017/9781009157896.020.

Harper, K. L., Lamarche, C., Hartley, A., Peylin, P., Ottlé, C., Bastrikov, V., ... & Defourny, P.: A 29-year time series of annual 300 m resolution plant-functional-type maps for climate models. *Earth System Science Data*, *15*(3), 1465-1499, 2023.

Krinner, G., Viovy, N., de Noblet-Ducoudré, N., Ogée, J., Polcher, J., Friedlingstein, P., Ciais, P., Sitch, S., and Prentice, I. C.: A dynamic global vegetation model for studies of the coupled atmosphere-biosphere system, *Global Biogeochemical Cycles, 19*, GB1015, doi:10.1029/2003GB002199, 2005.

Krinner, G., Derksen, C., Essery, R., Flanner, M., Hagemann, S., Clark, M., Hall, A., Rott, H., Brutel-Vuilmet, C., Kim, H., Ménard, C. B., Mudryk, L., Thackeray, C., Wang, L., Arduini, G., Balsamo, G., Bartlett, P., Boike, J., Boone, A., Chéruy, F., Colin, J., Cuntz, M., Dai, Y., Decharme, B., Derry, J., Ducharne, A., Dutra, E., Fang, X., Fierz, C., Ghattas, J., Gusev, Y., Haverd, V., Kontu, A., Lafaysse, M., Law, R., Lawrence, D., Li, W., Marke, T., Marks, D., Ménégoz, M., Nasonova, O., Nitta, T., Niwano, M., Pomeroy, J., Raleigh, M. S., Schaedler, G., Semenov, V., Smirnova, T. G., Stacke, T., Strasser, U., Svenson, S., Turkov, D., Wang, T., Wever, N., Yuan, H., Zhou, W., and Zhu, D.: ESM-SnowMIP: assessing snow models and quantifying snow-related climate feedbacks, *Geoscientific Model Development*, *11*, 5027–5049, https://doi.org/10.5194/gmd-11-5027-2018, 2018.

Luojus, K., Pulliainen, J., Takala, M., Lemmetyinen, J., Mortimer, C., Derksen, C., ... & Venäläinen, P.: GlobSnow v3.0 Northern Hemisphere snow water equivalent dataset. *Scientific Data*, *8*(1), 163, 2021.

Niu, G.-Y., and Yang, Z.-L: Effects of vegetation canopy processes on snow surface energy and mass balances, *Journal of Geophysical Research, 109*, D23111, doi:10.1029/2004JD004884, 2004.

Niu, G.-Y., and Yang, Z.-L.: An observation-based formulation of snow cover fraction and its evaluation over large North American river basins, *Journal of Geophysical Research, 112*, D21101, doi:10.1029/2007JD008674, 2007.

Pomeroy, J. W., & Brun, E.: Physical properties of snow. *Snow ecology: An interdisciplinary examination of snow-covered ecosystems*, *45*, 118, 2001.

Raoult, N., Charbit, S., Dumas, C., Maignan, F., Ottlé, C., and Bastrikov, V.: Improving modelled albedo over the Greenland ice sheet through parameter optimisation and MODIS snow albedo retrievals, *The Cryosphere, 17*, 2705–2724, https://doi.org/10.5194/tc-17-2705-2023, 2023.

Solberg, R., G. Schwaizer, T. Nagler, S. Wunderle, K. Naegeli, K. Luojus, M. Takala, J. Pulliainen, J. Lemmetyinen, and M. Moisander: ESA CCI+ Snow ECV: Product User Guide, version 3.1, December 2021, 2021.

Takala,M., Luojus, K., Pulliainen, J., Derksen, C., Lemmetyinen, J., Kärnä, J.-P., Koskinen, J. and Bojkov, B.: Estimating northern hemisphere snow water equivalent for climate research through assimilation of space-borne radiometer data and ground-based measurements, *Remote Sensing of Environment, Volume 115, Issue 12*, 15 December 2011, Pages 3517-3529. doi: 10.1016/j.rse.2011.08.014, 2011.

Vuichard, N., Messina, P., Luyssaert, S., Guenet, B., Zaehle, S., Ghattas, J., Bastrikov, V. and Peylin, P.: Accounting for carbon and nitrogen interactions in the global terrestrial ecosystem model ORCHIDEE (trunk version, rev 4999): Multi-scale evaluation of gross primary production. *Geoscientific Model Development, 12(11)*, 4751-4779, doi:10.5194/gmd-12-4751-2019, 2019.

Wang, T., Ottlé, C., Boone, A., Ciais, P., Brun, E., Morin, S., Krinner, G., Piao, S. and Peng, S.: Evaluation of an improved intermediate complexity snow scheme in the ORCHIDEE land surface model, *Journal of Geophysical Research Atmosphere, 118*, 6064–6079, doi:10.1002/jgrd.50395, 2013.

9. Glossary

Terms	
Data assimilation	Observations directly influence the model initial state considering their error characteristics during every cycle of a model. This is used for reanalysis, NWP, which includes seasonal and decadal forecasting.
Model validation	Observations are compared with equivalent model fields to assess the accuracy of the model. This can be on short time scales for process studies or long-time scales for climate trends.
Climate monitoring	This describes the use of a satellite only dataset to monitor a particular atmospheric or surface variable over a period > 15yrs to investigate whether there is a trend due to climate change.
Initialisation	To initialise prognostic quantities of the model with reasonable values at the beginning of the simulation but do not continuously update.
Prescribe boundary conditions	Prescribe boundary conditions for a model run for variables that are not prognostic (e.g. land cover, ice caps etc).
Accuracy	Accuracy is the measure of the non-random, systematic error, or bias, that defines the offset between the measured value and the true value that constitutes the SI absolute standard.
Stability	Stability is a term often invoked with respect to long-term records when no absolute standard is available to quantitatively establish the systematic error – the bias defining the time-dependent (or instrument-dependent) difference between the observed quantity and the true value.
Precision	Precision is the measure of reproducibility or repeatability of the measurement without reference to an international standard so that precision is a measure of the random and not the systematic error. Suitable averaging of the random error can improve the precision of the measurement but does not establish the systematic error of the observation.
Acronyms	
AR6	Assessment Report 6 (of the IPCC)
AVHRR	Advanced Very High-Resolution Radiometer
CCI	Climate Change Initiative
CMC	Climate Modelling Community
CMIP6/7	Climate Model Intercomparison Project-6/7
CMUG	Climate Modelling Users Group
ECV	Essential Climate Variable
EGU	European Geophysical Union
ENSO	El Nino- Southern Oscillation
ERA	ECMWF Reanalysis
IPCC	Intergovernmental Panel on Climate Change
LAI	Leaf Area Index
PMR	Passive Microwave Radiometer
SCF	Snow Cover Fraction
SCFG	Snow Cover Fraction Ground

SCFV	Snow Cover Fraction Viewable
SWE	Snow Water Equivalent
WGI	Working Group One

10. Appendix

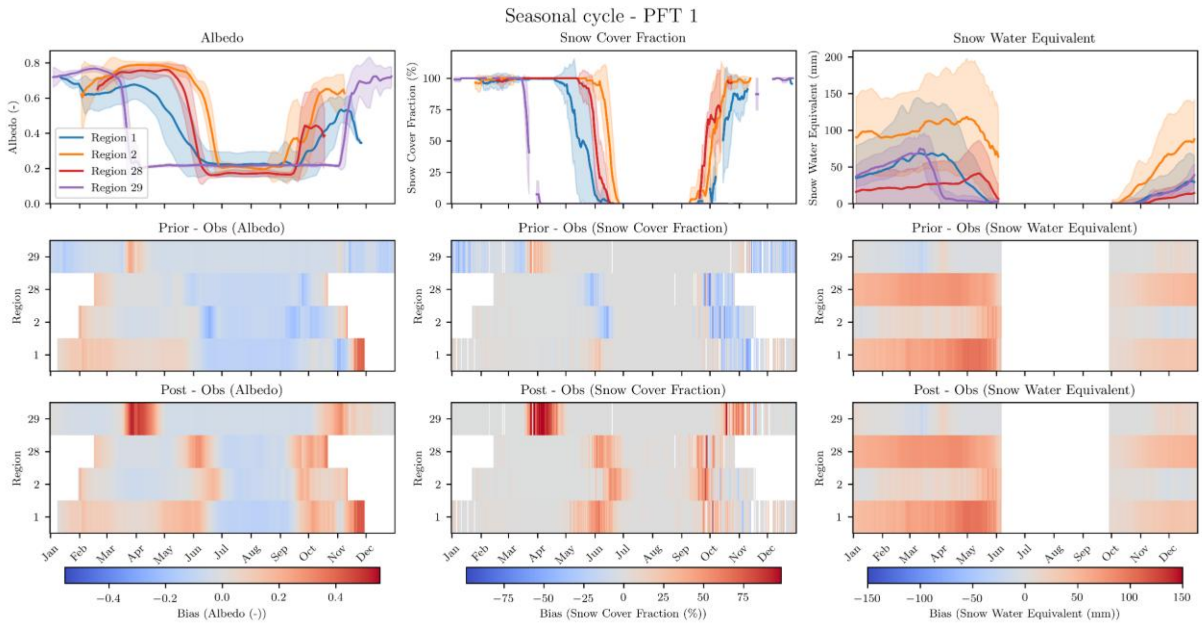
Seasonal cycle - PFT 1
Albedo
Snow Cover Fraction
Snow Water Equivalent
Albedo (-)
Snow Cover Fraction (%)
Snow Water Equivalent (mm)
Region 1
Region 2
Region 28
Region 29
Prior - Obs (Albedo)
Prior - Obs (Snow Cover Fraction)
Prior - Obs (Snow Water Equivalent)
Post - Obs (Albedo)
Post - Obs (Snow Cover Fraction)
Post - Obs (Snow Water Equivalent)
Region
Jan Feb Mar Apr May Jun Jul Aug Sep Oct Nov Dec
Bias (Albedo (-))
Bias (Snow Cover Fraction (%))
Bias (Snow Water Equivalent (mm))

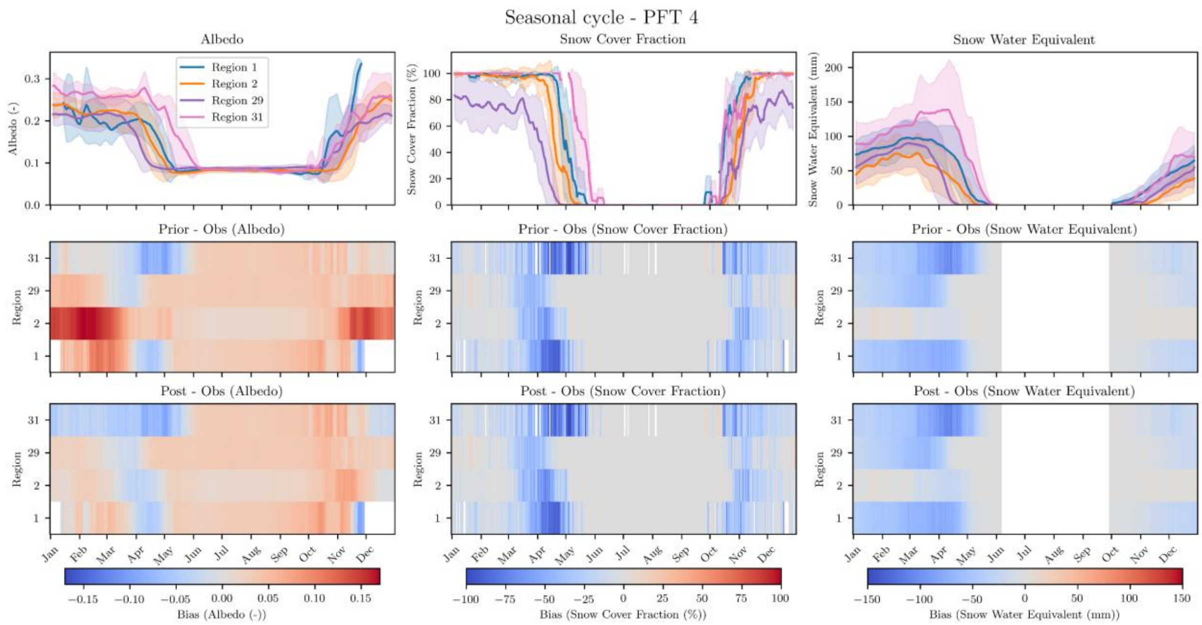
Seasonal cycle - PFT 4
Albedo
Snow Cover Fraction
Snow Water Equivalent
Albedo (-)
Snow Cover Fraction (%)
Snow Water Equivalent (mm)
Region 1
Region 2
Region 29
Region 31
Prior - Obs (Albedo)
Prior - Obs (Snow Cover Fraction)
Prior - Obs (Snow Water Equivalent)
Post - Obs (Albedo)
Post - Obs (Snow Cover Fraction)
Post - Obs (Snow Water Equivalent)
Region
Jan Feb Mar Apr May Jun Jul Aug Sep Oct Nov Dec
Bias (Albedo (-))
Bias (Snow Cover Fraction (%))
Bias (Snow Water Equivalent (mm))

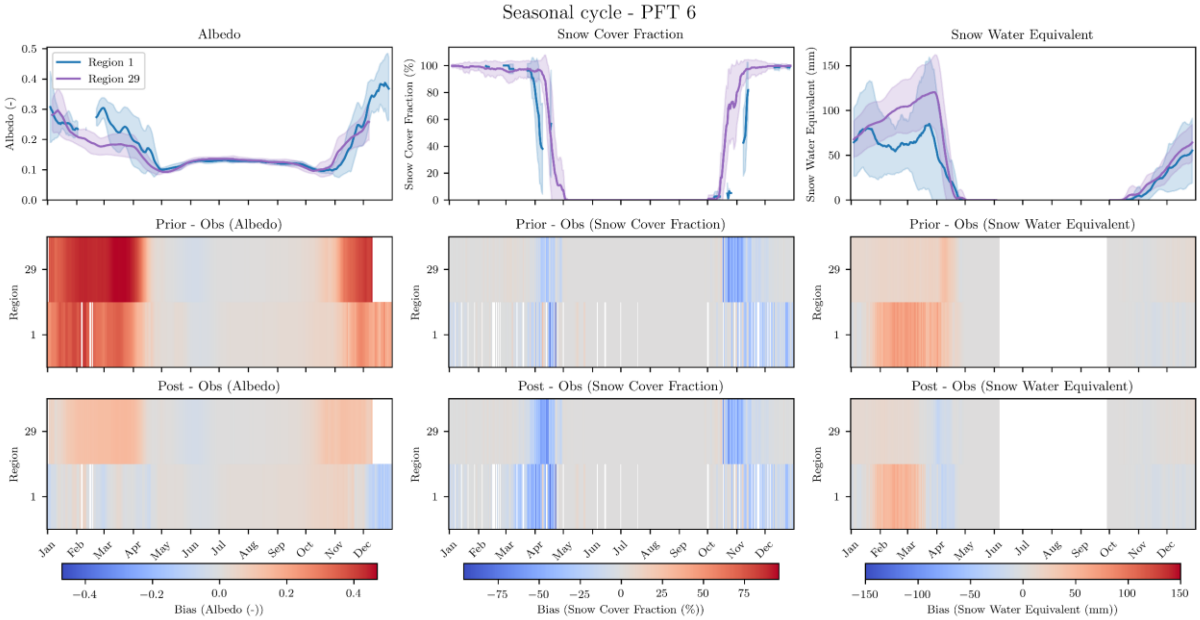
Seasonal cycle - PFT 6
Albedo
Snow Cover Fraction
Snow Water Equivalent
Region 1
Region 29
Prior - Obs (Albedo)
Prior - Obs (Snow Cover Fraction)
Prior - Obs (Snow Water Equivalent)
Post - Obs (Albedo)
Post - Obs (Snow Cover Fraction)
Post - Obs (Snow Water Equivalent)
Bias (Albedo (-))
Bias (Snow Cover Fraction (%))
Bias (Snow Water Equivalent (mm))

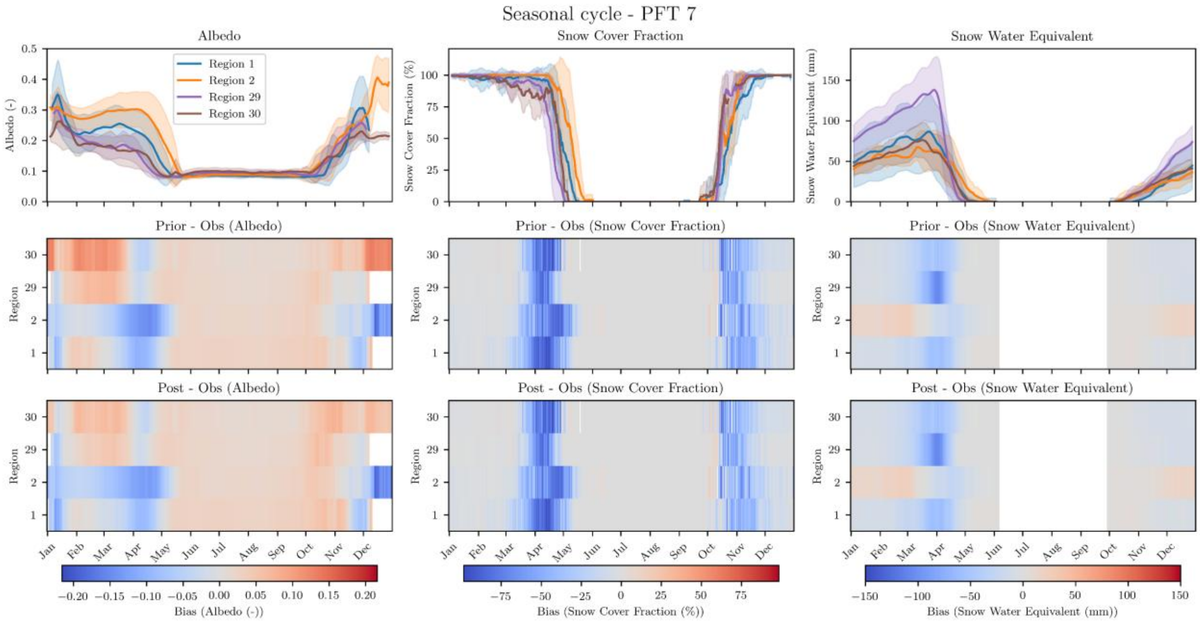
Seasonal cycle - PFT 7
Albedo
Snow Cover Fraction
Snow Water Equivalent
Region 1
Region 2
Region 29
Region 30
Prior - Obs (Albedo)
Prior - Obs (Snow Cover Fraction)
Prior - Obs (Snow Water Equivalent)
Post - Obs (Albedo)
Post - Obs (Snow Cover Fraction)
Post - Obs (Snow Water Equivalent)
Bias (Albedo (-))
Bias (Snow Cover Fraction (%))
Bias (Snow Water Equivalent (mm))

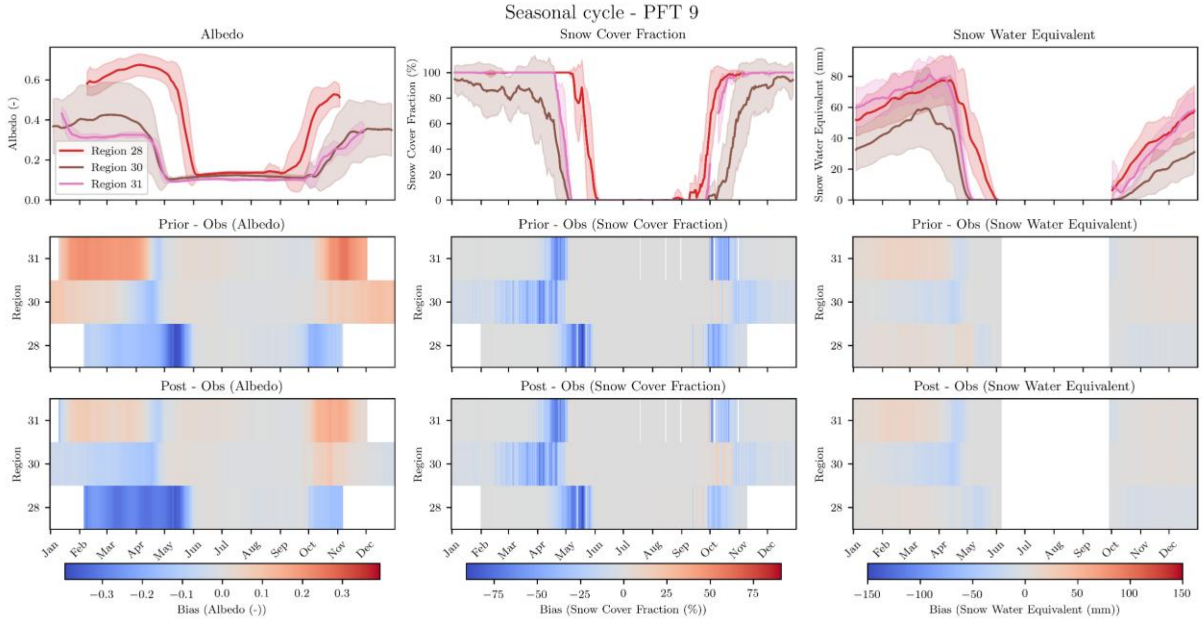
Seasonal cycle - PFT 9
Albedo
Snow Cover Fraction
Snow Water Equivalent
Region 28
Region 30
Region 31
Albedo (-)
Snow Cover Fraction (%)
Snow Water Equivalent (mm)
Prior - Obs (Albedo)
Prior - Obs (Snow Cover Fraction)
Prior - Obs (Snow Water Equivalent)
Post - Obs (Albedo)
Post - Obs (Snow Cover Fraction)
Post - Obs (Snow Water Equivalent)
Region
Jan Feb Mar Apr May Jun Jul Aug Sep Oct Nov Dec
Bias (Albedo (-))
Bias (Snow Cover Fraction (%))
Bias (Snow Water Equivalent (mm))

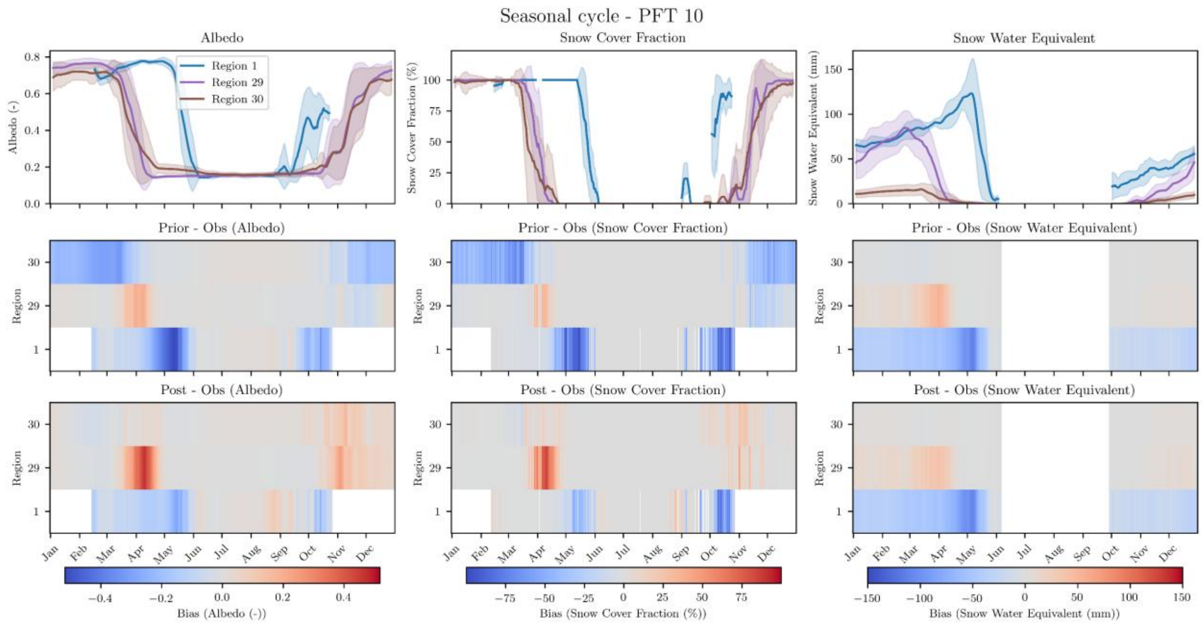
Seasonal cycle - PFT 10
Albedo
Snow Cover Fraction
Snow Water Equivalent
Region 1
Region 29
Region 30
Albedo (-)
Snow Cover Fraction (%)
Snow Water Equivalent (mm)
Prior - Obs (Albedo)
Prior - Obs (Snow Cover Fraction)
Prior - Obs (Snow Water Equivalent)
Post - Obs (Albedo)
Post - Obs (Snow Cover Fraction)
Post - Obs (Snow Water Equivalent)
Region
Jan Feb Mar Apr May Jun Jul Aug Sep Oct Nov Dec
Bias (Albedo (-))
Bias (Snow Cover Fraction (%))
Bias (Snow Water Equivalent (mm))

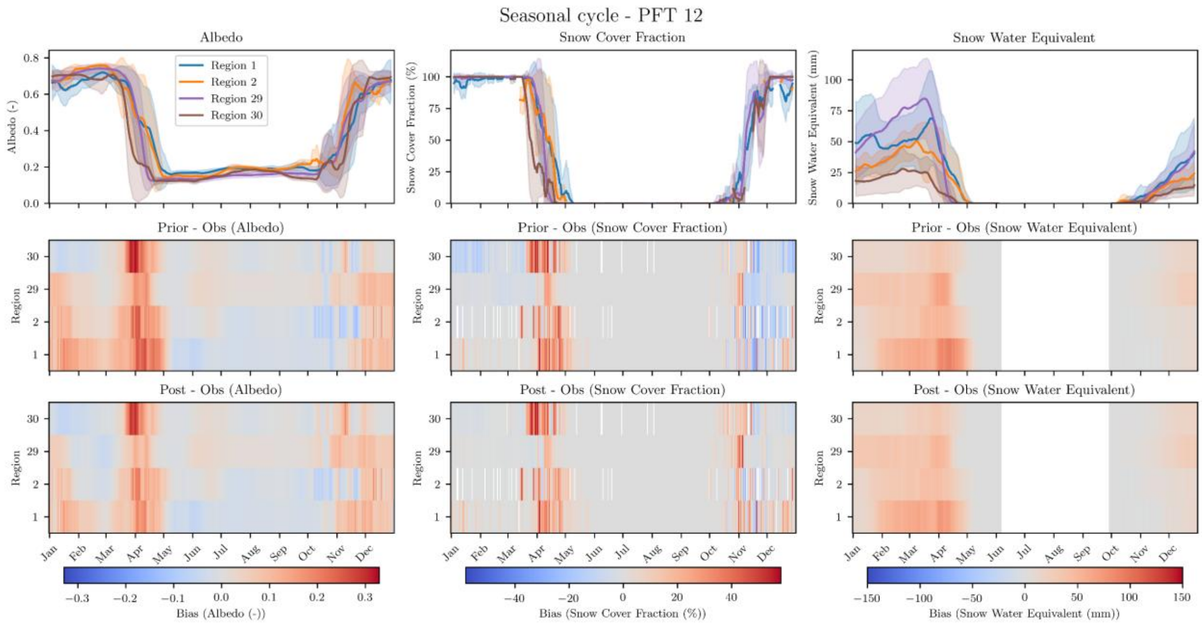
Seasonal cycle - PFT 12
Albedo
Snow Cover Fraction
Snow Water Equivalent
Region 1
Region 2
Region 29
Region 30
Albedo (-)
Snow Cover Fraction (%)
Snow Water Equivalent (mm)
Prior - Obs (Albedo)
Prior - Obs (Snow Cover Fraction)
Prior - Obs (Snow Water Equivalent)
Post - Obs (Albedo)
Post - Obs (Snow Cover Fraction)
Post - Obs (Snow Water Equivalent)
Region
Jan Feb Mar Apr May Jun Jul Aug Sep Oct Nov Dec
Bias (Albedo (-))
Bias (Snow Cover Fraction (%))
Bias (Snow Water Equivalent (mm))